LASER INTERFEROMETER GRAVITATIONAL WAVE OBSERVATORY
- LIGO -
CALIFORNIA INSTITUTE OF TECHNOLOGY
MASSACHUSETTS INSTITUTE OF TECHNOLOGY

Technical Note	**LIGO-T2100198–v1**	2021/10/25

Building blocks of a PT-symmetric interferometer

Student: Kagan Yanik
Mentors: Yanbei Chen, Rana Adhikari, Xiang Li, Shruti Jose Maliakal

California Institute of Technology
LIGO Project, MS 18-34
Pasadena, CA 91125
Phone (626) 395-2129
Fax (626) 304-9834
E-mail: info@ligo.caltech.edu

Massachusetts Institute of Technology
LIGO Project, Room NW22-295
Cambridge, MA 02139
Phone (617) 253-4824
Fax (617) 253-7014
E-mail: info@ligo.mit.edu

LIGO Hanford Observatory
Route 10, Mile Marker 2
Richland, WA 99352
Phone (509) 372-8106
Fax (509) 372-8137
E-mail: info@ligo.caltech.edu

LIGO Livingston Observatory
19100 LIGO Lane
Livingston, LA 70754
Phone (225) 686-3100
Fax (225) 686-7189
E-mail: info@ligo.caltech.edu

http://www.ligo.caltech.edu/

Abstract

In gravitational wave research, one of the challenges for conventional detectors is that we need to sacrifice peak sensitivity to obtain a larger bandwidth in the noise spectrum. White Light Cavities (WLC) enable us to improve the bandwidth without sacrificing the peak sensitivity. In our project, we consider a PT-symmetric interferometer consisting of an arm cavity, a test mass attached to the arm cavity, a filter cavity, and a mechanical oscillator which is the end mirror of the filter cavity. This interferometer with coherent quantum feedback yields a stabilized WLC (sWLC). However, the backaction noise due to radiation pressure on the test mass reduces the sensitivity of the system in the lower frequency range. In this project, we introduce an effective negative mass to cancel the backaction noise and obtain a larger bandwidth by sacrificing less of the sensitivity compared to a conventional detector. We achieve the negative mass by applying blue-detuned pumping, red-detuned pumping, and detuning to the filter cavity while also utilizing an additional optical mode inside it. We also simulate the optical spring effect of the filter cavity of the system in FINESSE.

1 Text

1.1 Introduction/Background

1.1.1 Bandwidth Sensitivity Trade-off

Conventional LIGO detectors (consisting of a Michelson interferometer) are subject to a trade-off between the bandwidth and the sensitivity of the detector. This trade-off is as a result of the Energetic Quantum Limit (EQL) which is represented by the inequality [1]

$$\int_0^{+\infty} d\Omega/(2\pi) S_h^{-1}(\Omega) \leq \Delta\mathcal{E}^2/(4\hbar)^2, \tag{1}$$

where S_h is the spectral density normalized for signal. If we want a larger bandwidth, we would have to sacrifice the peak sensitivity and for a sharper peak sensitivity, we would have a smaller bandwidth for the strain noise being detected, hence the trade-off.

1.1.2 White Light Cavity System

Our goal in this project is to overcome this bandwidth-sensitivity trade-off and sacrifice less of sensitivity for a broader bandwidth. To achieve that we want to build a White Light Cavity (WLC) that consists of an arm cavity with optical mode $\hat{a}$ (Michelson interferometer), a filter cavity with optical mode $\hat{b}$ (Fabry-Perot cavity) and the movable end mirror of the filter cavity (mechanical oscillator) with mechanical mode $\hat{c}$. In our WLC system, the arm cavity has normal dispersion where the input-output relation yields phase delay and the filter cavity has anomalous dispersion where the input-output relation implies non-causality. Since we often face technical complications with unstable WLC (uWLC) systems (where the input field is sent inside the arm cavity and the readout from the output field is also received from the arm cavity), we use a stabilized WLC (sWLC). To stabilize the system we will use a coherent quantum feedback with PT-symmetry where the input field is sent into the filter

cavity and the output field is the field reflected from the filter cavity from which the detector obtains the readout. This setup can be seen more clearly in FIG.2. Moreover, this system is PT-symmetric when $\chi = \kappa$.

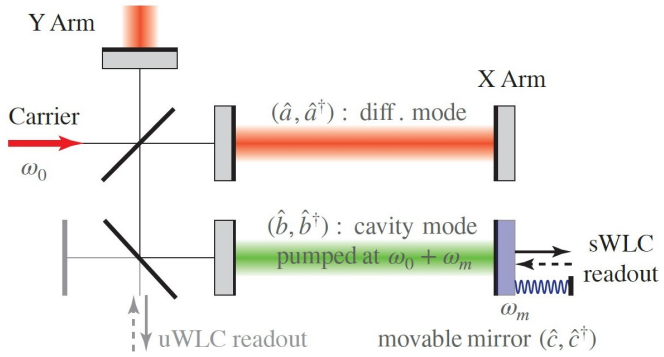

Figure 1: WLC setup [1] with arm cavity ($\hat{a}$), filter cavity ($\hat{b}$) with optical resonance frequency ω_0, and the filter cavity's movable end mirror ($\hat{c}$) with mechanical resonance frequency ω_m,

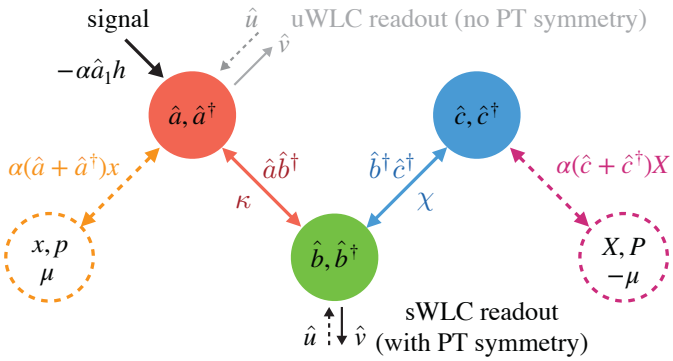

Figure 2: The stable White Light Cavity (sWLC) scheme [1]. The arm cavity has mode $\hat{a}$, the filter cavity has mode $\hat{c}$ and the detector has mode $\hat{b}$. Mode $\hat{a}$ couples to mode $\hat{b}$ with a coupling rate κ and mode $\hat{c}$ couples to mode $\hat{b}$ with coupling rate χ. Mode $\hat{b}$ is coupled to stable WLC (sWLC) readout. This system is PT symmetric when χ=κ. $\hat{u}$ is the input vacuum noise and $\hat{v}$ is the output field.

1.1.3 Anomalous Dispersion

In this sWLC system we observe dispersive optomechanical coupling between the filter cavity ($\hat{b}$) with blue-detuned pumping ($\omega_p = \omega_0 + \omega_m$) and the movable mirror ($\hat{c}$) where the mechanical oscillation due to weak signal force modulates the filter cavity's resonance frequency [8]. The mechanical oscillations of the mirror causes detuning in the cavity by causing microscopical changes in the filter cavity length. This change causes a shift in the resonant frequency of the cavity and we obtain the new resonance frequency:

$$\omega_b = \omega_0 + Gx, \tag{2}$$

where ω_0 is he initial filter cavity resonance frequency, $G = \omega_0/L_b$ is the coupling strength indicating the change in resonance frequency per unit length of the cavity, and x is the displacement of the movable mirror at a given time. This optomechanical interaction is expressed by the Hamiltonian

$$\hat{H}_{OM} = -\hbar G \hat{b}^\dagger \hat{b} \hat{x}, \tag{3}$$

where $\hat{x} = x_{ZPF}(\hat{c}^\dagger e^{i\omega_m t} + \hat{c}e^{-i\omega_m t})$ with $x_{ZPF} = \sqrt{\hbar/2m_c\omega_m}$ being the zero point fluctuation. Using linearization, rotating wave approximation with frequency matching condition ($\omega_p = \omega_0 + \omega_m$), and expressing G in terms of χ shown in FIG.1, we express the optomechanical coupling as

$$\hat{H}_{OM} = i\hbar\chi(\hat{b}^\dagger\hat{c}^\dagger - \hat{b}\hat{c}). \tag{4}$$

Then, the interaction Hamiltonian (interaction between $\hat{a}-\hat{b}$ and between $\hat{b}-\hat{c}$) is expressed as

$$\hat{V}_{\text{int}} = i\hbar\kappa(\hat{a}\hat{b}^\dagger - \hat{a}^\dagger\hat{b}) + i\hbar\chi(\hat{b}^\dagger\hat{c}^\dagger - \hat{b}\hat{c}), \tag{5}$$

where κ is the coupling rate between $\hat{a}-\hat{b}$. From the optomechanical interaction Hamiltonian $\hat{H}_{OM}$, we can see the anomalous dispersion relation between input and output fields of the filter cavity. To obtain this relation, we use the Heisenberg picture on this Hamiltonian to obtain the equations of motion for $\hat{b}$ and $\hat{c}^\dagger$, then applied Fourier transform to get the equations in the frequency domain and then added dissipation for losses. Since the output field is $\hat{v} = \hat{u} - \sqrt{2\gamma_r}\hat{b}$, the anomalous dispersion (phase advance of the output field compared to the input field) can be shown by the following relation

$$\hat{v}(\Omega) = \frac{\Omega + i\gamma_{opt}}{\Omega - i\gamma_{opt}}\hat{u}(\Omega), \tag{6}$$

where Ω is the sideband frequency around the resonance frequency of the filter cavity, ranging from 10 to 10^4 Hz, γ_{opt} is the negative mechanical damping rate due to optomechanical interaction [2]. While a normal cavity exhibits positive dispersion for this input-output relation, a passive filter cavity exhibits negative dispersion [2]. In this relation we have assumed that the cavity bandwidth $\gamma_f >> \Omega$, and $\gamma_{opt} >> \gamma_m$ (mechanical damping rate).

1.1.4 Backaction

Gravitational waves apply a classical signal force on the movable mirror (a test mass that can be considered as a mechanical oscillator) of the cavity and causes displacement of the mirror. Since the displacement of the mirror changes the length of the cavity, this creates very small variations in the phase of the field. Hence, the displacement can be read out from the phase of the optical field. Simultaneously, the amplitude fluctuations of the optical field provide an additional backaction force on the mirror which drives the momentum of the mirror. As a result, the position of the mirror also changes and the phase shift of the optical field due to this force indicates the backaction noise. The motion of the test mass mirror under radiation pressure due to GW is expressed by the Hamiltonian [1]:

$$\hat{V}_{GW} = \alpha_{GW}(\hat{x} - L_a h)\hat{a}_1 + \frac{\hat{p}^2}{2\mu}, \tag{7}$$

where $\alpha_{GW} = \sqrt{2P_c\hbar\omega_0/(L_a c)}$ is the radiation pressure force per photon, P_c is the circulating power inside arm cavity, and L_a is the length of arm cavity.

The backaction noise will increase when we increase the pumping power of the laser. In our project, we observe backaction when the strong field interacts with the test mass μ with mode $(\hat{x}, \hat{p})$ attached to the arm cavity (mode $\hat{a}$). Due to backaction, both the conventional and any WLC noise spectra have a tail at low frequencies [1] where radiation pressure noise is effective, which can be seen in FIG. 3.

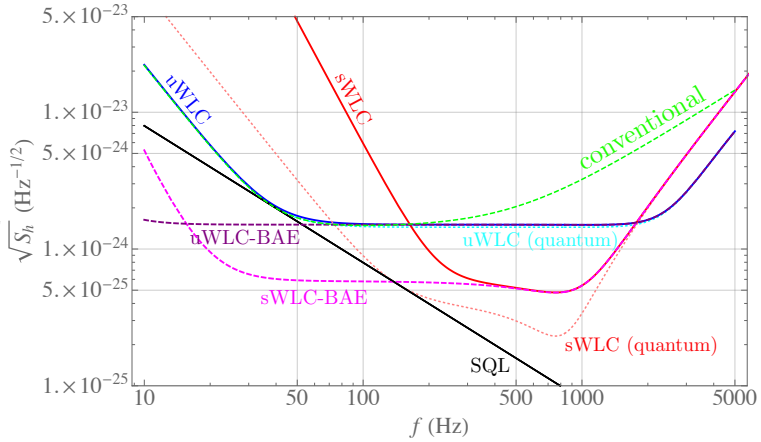

Figure 3: GW noise spectra for sWLC and uWLC both with and without backaction evasion (BAE) [1]. We can see that the tails of uWLC and sWLC at low frequencies have been flattened more due to backaction evasion.

In this project, our objective is to add back-action evasion module to realize the full PT-symmetric structure of FIG. 2 which has not been described in prior work [1]. To preserve the PT-symmetry structure of the system, (since $\hat{a}$ and $\hat{c}$ are PT-symmetric) we aim to attach another mode $(\hat{X}, \hat{P})$ with negative mass $-\mu$ to mode $\hat{c}$. The P-symmetry is done by attaching (X,P) to $\hat{c}$ and T-symmetry is preserved by the negative mass since $\dot{X} = \frac{P}{-\mu}$. Conserving the PT-symmetry of the system causes backaction evasion, which flattens the tails of uWLC and sWLC noise spectrum curves at low frequencies.

2 Methods

2.1 Negative Mass

The complete description of the system includes the optomechanical interaction between test mass $(\hat{x}, \hat{p})$ and the cavity mode $\hat{a}$. The total Hamiltonian is given by

$$\hat{H} = \hat{V}_{\rm GW} + \hat{V}_{\rm int}, \tag{8}$$

where μ is the reduced mass of the cavity mirrors, and $\hat{V}_{\rm int}$ is given previously where the PT-symmetry was initially constructed by adding a filter cavity to the arm cavity. Considering the interaction between mode $\hat{a}$ and the test mass $(\hat{x}, \hat{p})$, the PT-symmetry is no longer reserved. To restore the PT-symmetry of the system, we need to add a negative mass

counterpart and attach it to mode $\hat{c}$:

$$\hat{V}_{\rm aux} = \alpha(\hat{c} + \hat{c}^\dagger)X + \frac{\hat{P}^2}{-2\mu}. \tag{9}$$

Attaching $(\hat{X}, \hat{P})$ to mode $\hat{c}$ will conserve the P-symmetry, while the negative mass will conserve the time reversal symmetry.

To implement this negative mass in our system, we propose to add an optomechanical auxiliary mode ($\hat{d}$, $\hat{d}^\dagger$), which is expressed by the Hamiltonian

$$\hat{V}_{\rm aux} = -\hbar\alpha_d X^{\rm d}_{\rm ZPF}\hat{c}_1\hat{d}_1 - \hbar\omega_d\hat{d}^\dagger\hat{d} \tag{10}$$

with $X^{\rm d}_{\rm ZPF} = \sqrt{\hbar/(2\mu\omega_d)}$ and ω_d being the fictitious mechanical resonant frequency. $\alpha_d = \omega_{p1}/L_d$ is the dispersive coupling strength of the interaction, $\hat{c}_1$ and $\hat{c}_1$ are the amplitude quadratures of modes $\hat{c}$ and $\hat{d}$.

Besides this optomechanical system, other realizations such as a nonlinear crystal realization can potentially achieve similar results.

2.2 Mathematica Simulation for BAE

We first simulated the effect of backaction evasion on the GW noise spectra by using the LIGO Voyager parameters [1]. The simulation considers three noise sources: shot noise dominant at higher frequencies, backaction noise (from GW-test mass interaction) and thermal noise (from the thermal bath attached to the mechanical mode $\hat{c}$) [4] dominant at lower frequencies. In this simulation, we compare the four cases of sWLC with the conventional detector which consists of single arm cavity with a test mass attached to it. From FIG.4, we can see that for BAE with no thermal noise (a noise source dominant at lower frequencies), we achieve a broader bandwidth with much better sensitivity than the conventional detector. FIG.4 also shows that sensitivity is improved at lower frequencies when BAE is achieved with negative mass compared to when there is backaction noise present. We simulate these results from a theoretical point based on Eq.9 without any characterization or physical realization of negative mass.

2.3 Achieving Negative Mass Hamiltonian

In this project, we aim to cancel the backaction noise resulting from the radiation pressure force on the test mass attached to the arm cavity. To achieve BAE we aim to attach to mode $\hat{c}$ (mechanical oscillator) an auxiliary optical mode $(X, P) \sim (\hat{d}, \hat{d}^\dagger)$ with effective negative mass $-\mu$, in order to achieve the (effective) Hamiltonian in Eq.10.

where α_d is proportional to the dispersive coupling constant between $\hat{c}$ and $\hat{d}$, $x^{\rm ETM}_{\rm ZPF}$ is the zero point fluctuation of the effective test mass of the mechanical oscillator. Based on the Hamiltonian we realized that we need blue and red-detuned pumping and detuning. We derived the necessary expressions to characterize the power required for both pumping and how much detuning we need from the resonant frequency of the optical mode $\hat{d}$ (ω_D).

Parameter	Value
γ_R	$(2\pi)500$ Hz
Q	$8\text{x}10^9$
κ	$(2\pi)5000$ Hz
χ	$(2\pi)5000$ Hz
k_B	$1.38065\text{x}10^{-23}$ $m^2s^{-2}kgK^{-1}$
T	4 K
μ	50 kg
μc	-50 kg
ω_m	$(2\pi)10$ kHz
ω_0	$(2\pi)299792458$ $ms^{-1}/2\mu m$
$\hbar$	$1.054571628\text{x}10^{-34}$ Js
L_{arm}	4000 m
c	299792458 ms^{-1}
P_c	$3\text{x}10^6$ Watt

Table 1: LIGO Voyager parameters [1] used in GW Noise Spectra.

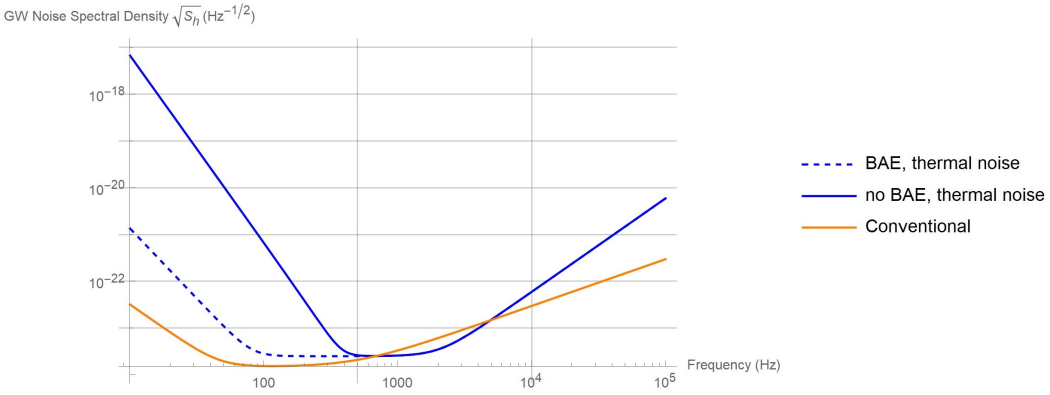

Figure 4: Normalized noise spectral density for the three cases mentioned previously for the parameters $\gamma_R = 2\pi(500)Hz, \gamma_m = 2\pi\omega_m/(2Q)Hz$ or $0Hz$ (depending on the case), $\kappa = \chi = 10\gamma_R, L = 4000m, -\mu_c = \mu = 50kg, T = 273K, \omega_m = 10kHz$, Q=$8\text{x}10^9$.

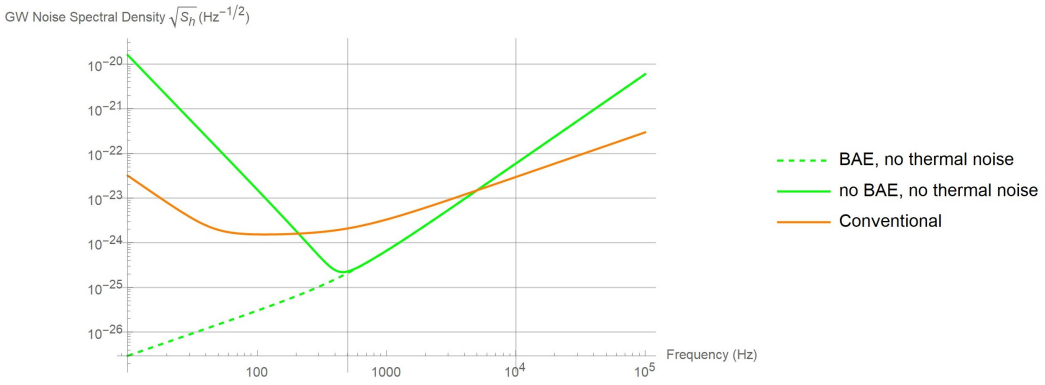

Figure 5: Normalized noise spectral density for the three cases mentioned previously for the parameters $\gamma_R = 2\pi(500)Hz, \gamma_m = 2\pi\omega_m/(2Q)Hz$ or $0Hz$ (depending on the case), $\kappa = \chi = 10\gamma_R, L = 4000m, -\mu_c = \mu = 50kg, \omega_m = 10kHz$, Q=8x10^9.

2.3.1 PI/BS interaction

Parametric interaction and beam splitter interaction happen as a result of blue-detuned pumping and red-detuned pumping respectively. These are achieved as a result of the interaction between the mechanical oscillator $\hat{c}$ and the optical mode $\hat{d}$ of the negative mass inside filter cavity. This corresponds to the first term of the Hamiltonian in Eq.10. In the mechanical rotating frame we express the coupling Hamiltonian between $\hat{c}$ and $\hat{d}$ as

$$\begin{aligned}\hat{V}_{\mathrm{PI/BS}} = \alpha_d x^{\mathrm{c}}_{\mathrm{ZPF}}(\hat{c}e^{-i\omega_m t} + \hat{c^\dagger}e^{i\omega_m t})(D_1 e^{-i\omega_{p1}t} + D_2 e^{-i\omega_{p2}t} + \hat{d}e^{-i\omega_D t}) \\ (D_1 e^{i\omega_{p1}t} + D_2 e^{i\omega_{p2}t} + \hat{d^\dagger}e^{i\omega_D t}).\end{aligned} \tag{11}$$

The frequency match condition for blue and red-detuned pumping are $\omega_{p1} = \omega_D + \omega_m$ and $\omega_{p2} = \omega_D - \omega_m$ respectively. Applying these conditions to Eq.11, we get

$$\hat{V}_{\mathrm{PI/BS}} = \alpha_d x^{\mathrm{c}}_{\mathrm{ZPF}}(D_1(\hat{c}\hat{d} + \hat{c^\dagger}\hat{d^\dagger}) + D_2(\hat{c^\dagger}\hat{d} + \hat{c}\hat{d^\dagger})). \tag{12}$$

Since we aim to cancel the backaction in the Hamiltonian, we need to satisfy the following relation:

$$\alpha_d x^{\mathrm{c}}_{\mathrm{ZPF}} D_1 = \alpha x^{\mathrm{ETM}}_{\mathrm{ZPF}} \tag{13}$$

where $\alpha = \sqrt{2P_c\hbar\omega_0/L_a c}$ and $x^{\mathrm{ETM}}_{\mathrm{ZPF}} = \sqrt{\hbar/2\mu\omega^{\mathrm{ETM}}_m}$. Taking D_1 as the cavity mode amplitude, we get the following expression for the relation

$$\frac{\hbar\omega_{p1}}{L_d}\sqrt{\frac{\hbar}{2m_c\omega_m}}\sqrt{\frac{P_1 L_d}{2\pi\hbar\omega_{p1}c}} = \alpha X^{\mathrm{d}}_{\mathrm{ZPF}} \tag{14}$$

where m_c and ω_m are the mass and angular frequency of the oscillator respectively, P_1 and $\omega_{p1} = \omega_D + \omega_m$ are the power and angular frequency of blue-detuned pumping respectively. We took $\alpha_d = \hbar\omega_{p1}/L_d$ where ω_{p1}/L_d is the dispersive coupling strength of the interaction. From Eq.14, we can derive the expression to characterize the pumping power to achieve

blue-detuned pumping:

$$P_1 = 4\pi\left(\frac{L_d}{L_a}\right)\left(\frac{m_c}{\mu}\right)\left(\frac{\omega_m}{\omega_d}\right)\left(\frac{\omega_0}{\omega_{p1}}\right)P_c \tag{15}$$

where P_c is the power at the arm cavity and L_a is the arm cavity length. Same expression can be found for the red-detuned pumping by changing P_1 to P_2 and ω_{p1} to ω_{p2}. Assuming that $L_d = 300m, L_a = 4000m, m_c = 10^{-7}kg, \mu = 50kg$, ω_m has the same order of magnitude as ω_d and ω_0 has the same order of magnitude as ω_{p1}, P_1 is smaller than the circulating power P_c by nine orders of magnitude.

2.3.2 Detuning

Another pumping is done at an angular frequency (ω_{p0}) near the resonant frequency (ω_d) of $\hat{d}$ which is detuned by angular frequency Δ ($\omega_{p0} = \omega_d + \Delta$). This is achieved by the terms $\hat{d}\hat{d}^\dagger$ and $\hat{d}^\dagger\hat{d}$ which are present in the momentum operator of the Hamiltonian in Eq.10. Hence, for detuning, we get the following Hamiltonian

$$\hat{V}_{\text{det}} = \hbar\frac{\hbar}{8\mu(x_{\text{ZPF}}^{\text{ETM}})^2}(-\hat{d}\hat{d}^\dagger - \hat{d}^\dagger\hat{d}). \tag{16}$$

Using the conjugate pair relation $[\hat{d}, \hat{d}^\dagger]$=1, we simplify the Hamiltonian to

$$\hat{V}_{\text{det}} = \hbar\frac{\hbar}{-4\mu(x_{\text{ZPF}}^{\text{ETM}})^2}(\hat{d}^\dagger\hat{d} + \frac{1}{2}). \tag{17}$$

Ignoring the vacuum component of the Hamiltonian we can express its coefficient by equating the Hamiltonian to the detuning component of the quantum harmonic oscillator Hamiltonian $\hbar\Delta\hat{d}^\dagger\hat{d}$. Hence, we get the relation

$$\Delta = \frac{\hbar}{-4\mu(x_{\text{ZPF}}^{\text{ETM}})^2}. \tag{18}$$

For $x_{\text{ZPF}}^{\text{ETM}} = \sqrt{\frac{\hbar}{2\mu\omega_m^{\text{ETM}}}}$, we get the relation

$$\Delta = -\frac{\omega_m^{\text{ETM}}}{2}, \tag{19}$$

where $\omega_m^{\text{ETM}} \approx 1$Hz is the resonant frequency of arm cavity test mass.

2.4 Filter Cavity in FINESSE

We have worked on FINESSE [9] to simulate the filter cavity (mode $\hat{b}$) and show the anomalous dispersion. While most of the FINESSE code is completed towards simulating the cavity, there are some parameters and issues that remain to be fixed.

We started with the basics of the filter cavity by simulating a simple Fabry-Perot (FP) cavity with a fixed input mirror and a movable end mirror and applied a blue-detuned laser [9]. For

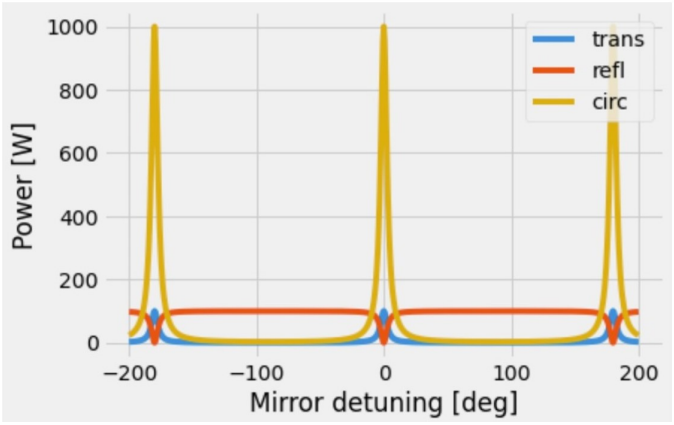

Figure 6: Circulating, reflected and transmitted power for varying detuning of the input mirror. Laser power is 100 W, cavity length is 4 m.

the FP cavity, we have shown in FIG. 7 that the resonance condition works by looking at the circulating, reflected and transmitted power at varying detuning of the input mirror since we get peak transmitted and circulating power and minimum reflected power at every 180 degree detuning.

We then checked the FP cavity without laser detuning to check the mechanics of the FP cavity by applying a mechanical transfer function to both mirrors [9]:

$$\chi_m(\Omega) = \frac{1}{m(\Omega^2 - \omega_m^2 + i\Omega\gamma_m)}, \tag{20}$$

where m is the mass of the mirror. In this case, we only see a single peak in the displacement of both mirrors, which shows the mechanical resonance frequency at $(2\pi)1$ Hz.

The circulating power as a function of the mirror detuning in FIG. 7 also demonstrates the optical spring effect (optically induced rigidity). For positive detuning (positive displacement), (since we have blue-detuned pumping) we see that the resonance frequency shifts. Since we have the relation,

$$K_{OS} = -\frac{dF_{opt}}{dx} \tag{21}$$

for the optical spring component of the spring constant, we see that $K_{OS} > 0$, and hence the optical resonance frequency is

$$\omega_{OS} = \sqrt{\frac{2P_c}{m\lambda_0}\frac{\Delta}{\Delta^2 + \gamma^2}} \tag{22}$$

where Δ is detuning and $\gamma = c\pi/(-L_b \ln(R^2))$ is the linewidth (R is the intensivity of the mirrors). This shows that the spring constant becomes more rigid:

$$K_{eff} = K + K_{OS} \tag{23}$$

where $K = m\omega_m^2$ and $K_{OS} = m\omega_{OS}^2$. Therefore, we expect a shift in the resonance frequency of the movable mirror equal to

$$\omega = \sqrt{\omega_m^2 + \omega_{OS}^2}. \tag{24}$$

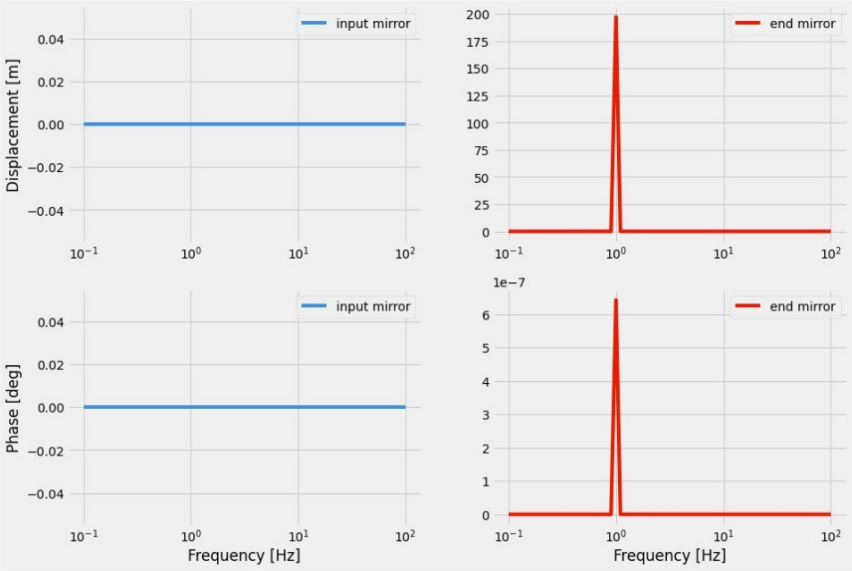

Figure 7: Displacement (upper) of input mirror (upper left) and end mirror (upper right) vs signal force frequency in linear-log scale. Relative phase to the force signal for both mirrors in logarithmic (lower left) and linear scale (lower right). Cavity is not detuned. Laser power is 3100 W, L_b=50 m, $\omega_m = (2\pi)1$ Hz, m=1 kg, Q_m=8x10^5.

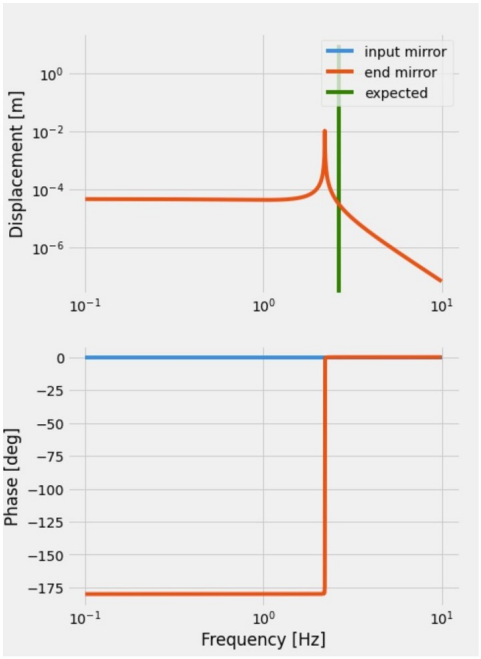

Figure 8: Displacement and phase of the end mirror vs signal force frequency in logarithmic scale (up) and linear-log scale (down). Cavity is detuned by $(2\pi)300$ Hz. Laser power is 3100 W, L_b=50 m, $\omega_m = (2\pi)1$ Hz, m=1 kg, Q_m=8x10^5, R=0.954. The green vertical line is the expected value from Eq. 24.

To show this optical spring effect, we checked the mechanical response of the oscillator for blue-detuned pumping to see the optical spring effect causing a shift in mechanical resonance frequency in FINESSE [9].

From FIG. 8, we can see that the resonance frequency indeed shifts to the right from $(2\pi)1$ Hz, but less than expected (the green line) as it does not exactly match the expected value.

For the next steps of our project, we aim to correct the problems with the FINESSE code to simulate the filter cavity, show the anomalous dispersion phase plots, input-output relations and compare them with the expected results. After that, we will be coupling the arm cavity to the filter cavity in FINESSE. We will also be evaluating how losses in any given mirrors of the arm and filter cavity and how they affect the input-output relations and noise spectrum.

For the effective negative mass, by using the right parameters, we will be calculating the power necessary for each pumping and detuning to realize the effective negative mass, design figure of merit and numerically optimize for the Hamiltonian we have for the negative mass. We will also be simulating the negative mass in Finesse.

References

[1] Li, Xiang, et al, *Broadband sensitivity improvement via coherent quantum feedback with PT symmetry*. arXiv preprint arXiv:2012.00836 (2020).

[2] Miao, Haixing, et al, *Enhancing the Bandwidth of Gravitational-Wave Detectors with Unstable Optomechanical Filters*. Phys. Rev. Lett. 115, 211104

[3] Chen, Yanbei, *Macroscopic quantum mechanics: theory and experimental concepts of optomechanics*. Journal of Physics B: Atomic, Molecular and Optical Physics 46.10 (2013): 104001.

[4] Li, Xiang, et al, *Supplementary Material for Broadband sensitivity improvement via coherent quantum feedback with PT symmetry*.

[5] Tsang, Mankei and Caves, Carlton M. *Evading quantum mechanics*. arXiv preprint arXiv:1203.2317 (2012).

[6] Khalili, F. Ya. and Polzik, E. S. *Overcoming the Standard Quantum Limit in Gravitational Wave Detectors Using Spin Systems with a Negative Effective Mass*. Phys. Rev. Lett. 121, 031101

[7] Arai, Koji, *Gravitational wave detection with laser interferometers*. LIGO SURF 2021 Lecture Presentation.

[8] Li, Xiang, et al, *Coherent coupling completing an unambiguous optomechanical classification framework*.

[9] A Freise, G Heinzel, H Lück, et al. Frequency domain interferometer simulation with higher-order spatial modes. *Classical and Quantum Gravity*, 21(5):S1067–S1074, 2004. Finesse is available at http://www.gwoptics.org/finesse.

3 Acknowledgments

I would especially want to thank Xiang Li and Shruti Jose Maliakal for their help and mentorship on this project. I would also like to thank Professor Yanbei Chen for his insights, suggestions and guidance and Professor Rana Adhikari for his feedback.

I am very grateful for the Simons Foundation (Award Number 568762), NSF, LIGO SURF Program, Caltech SFP funding, and Alan Weinstein who allowed me to have this research experience.